Precision Engineering 40 (2015) 55–73

Contents lists available at ScienceDirect

Precision Engineering

journal homepage: www.elsevier.com/locate/precision

A shearlet-based separation method of 3D engineering surface using high definition metrology

Shichang Du[a,b,*], Changping Liu[a], Delin Huang[a]

[a] Department of Industrial Engineering and Management, School of Mechanical Engineering, Shanghai Jiaotong University, Shanghai 200240, PR China
[b] State Key Laboratory of Mechanical System and Vibration, Shanghai 200240, PR China

ARTICLE INFO

Article history:
Received 7 November 2013
Received in revised form
16 September 2014
Accepted 4 October 2014
Available online 14 October 2014

Keywords:
Shearlet
3D engineering surface
Multi-scale geometric analysis
High definition metrology
Surface texture analysis

ABSTRACT

The 3D engineering surfaces are considered as having a range of spatial frequency components including roughness, waviness and form. Before the characterization of a 3D engineering surface, filtering is done first to separate these different components. To overcome the shortcomings of the traditional filtering methods, this paper presents a shearlet-based separation method using high definition metrology (HDM) that has the ability to measure a huge number of data points to represent a 3D surface. The 3D engineering surface is decomposed into different sub-bands of coefficients with non-subsampled shearlet transform (NSST). Then the surface components at different levels are reconstructed by applying an inverse NSST on the shearlet coefficients and combined into the above three surface components. The performance of the proposed method is validated by both simulated surface data and real-world 3D surface data, and the results demonstrate that the proposed shearlet-based method is effective for the separation and extraction of different surface components.

1. Introduction

The analysis of surface texture has gained more and more importance in the fields of mechanical manufacturing during recent years, since the functional behavior of a machined part is influenced by its surface texture. Additionally, the analysis of surface texture is considered as an important element in providing feedback on the manufacturing process. The relationship between surface texture, part functionality, and manufacturing process is the main reason for the description and analysis of surface texture.

The surface texture on an engineering surface is defined to have three components from the smaller to the larger scale: roughness, waviness and form. It is well recognized that different components have different impacts on the functional performance of the parts. To be specific, roughness reveals the irregularities on a surface left after manufacturing thus can be used to detect errors in the material removal process, also it has great impact on the part functionality such as friction and wear. Waviness, which may be generated by the vibration of the manufacturing system, has influence on the vibration resistance and tightness of the parts. The form, produced by the poor performance of the machine, can directly affect the assembling of the parts. Therefore, the motivation for classifying the above three components derives from the fact that roughness, waviness and form have different origins and affect part functionality in different ways. Separating a surface profile into different frequency components is of great significance and an important aspect of surface texture analysis.

Digital filtering is a common practice to realize the above separation process. Filtering of engineering surface has been a hot research topic since it is an important tool for surface texture analysis. Recent advances in filtering techniques are reviewed by Raja et al. [1]. The traditional filtering methods such as 2RC filter and Gaussian filter are firstly studied, and the Gaussian filter is the most widely used standard filtering technique [2]. However, it is well known that the Gaussian filter causes excessive distortion called "end effect" at the boundaries of the surface profile. Besides, it is not robust against outliers. To solve these problems, on the one hand, some modified methods based on Gaussian filter like regression and robust regression Gaussian filters [3] are proposed, on the other hand, some newer filtering methods like spline filter [4], robust spline filter [5], morphological filter [6] and wavelet-based filters [7,8] are proposed.

A comprehensive comparison of the above methods has been made by Raja et al. [9], and wavelet-based filtering is considered to be a very active research topic and has been barely scratched the tip of the iceberg. Different from the previous filtering

* Corresponding author at: Department of Industrial Engineering and Management, School of Mechanical Engineering, Shanghai Jiaotong University, Shanghai 200240, PR China. Tel.: +86 13764479720.
E-mail addresses: lovbin@sjtu.edu.cn, shichangdu@gmail.com (S. Du).

http://dx.doi.org/10.1016/j.precisioneng.2014.10.004
0141-6359/

methods, wavelet-based filters can provide multi-scale analysis, due to the reason that they can divide a given surface profile into different frequency components and study each component with a resolution matched to its scale. Hence, wavelet-based filters are not limited to separate the surface profile into three components (roughness, waviness and form), they can separate the profile into fine bandwidths that better reflect the changes of a manufacturing process. In recent years, several researchers have developed wavelet techniques and applied them to analyze engineering surfaces. Fu et al. [10] compared different wavelet bases and recommended Bior6.8 and Coif4 due to their transmission characteristics of the corresponding filters. Jiang et al. [11] developed a lifting wavelet representation for surface characterization, and different frequency components of the surface can be extracted according to the intended requirements of functional analysis. Josso et al. [12] proposed a frequency normalized wavelet transform for surface roughness analysis and characterization.

However, it is worth noting that, in most of the previous work, the engineering surfaces are characterized and analyzed with two-dimensional (2D) parameters since the stylus profilometer was invented in 1930s and widely used since then. Nevertheless, the 2D parameters are inadequate or incapable to characterize the surface texture in three dimensions (3D). With the rapid development of 3D measurement technology, a variety of sophisticated devices and techniques that have been developed and applied for 3D measurement of engineering surfaces. For example, a novel measurement technology called non-contact high definition metrology (HDM) has been adopted for 3D inspection of an entire surface as HDM can generate a surface height map of millions of data points within seconds [13]. In light of this, more appropriate surface characterization methods have been developed to obtain adequate information about 3D surface texture. Blunt and Jiang [14] have made efforts in extending the 2D parameters to characterize 3D surface, and the ASME B46.1 (American Society of Mechanical Engineers 2002) has also included some 3D parameters in its standard [15].

Likewise, it is necessary that the one-dimensional wavelet-based filter techniques are reasonably extended to two-dimensional ones. The discrete wavelet transform (DWT) is a widely used wavelet method in digital signal and image analysis, and it can be easily extended from one dimension to the condition of two dimensions. The application of 2D DWT in analyzing 3D engineering surfaces can be found in [16,17]. Zeng et al. [18] adopted two-dimensional dual-tree complex wavelet transform (2D DT-CWT) to separate engineering surfaces, which is more superior to 2D DWT in the aspects of shift-invariance and directional selectivity. However, both 2D DWT and 2D DT-CWT are fixed on directions. In other words, they both have only a few directions, which impair their performance in the filtering of 3D surfaces. In order to overcome the limitation of traditional 2D wavelets, the directional sensitivity should be increased. In light of this, a theory called multi-scale geometric analysis (MGA) has been proposed and is suitable to analyzing 3D surfaces. Recently, a new MGA tool called shearlets [19] was proposed. From the view of approximation theory, shearlets form a Parseval frame of well-localized waveforms at various scales and directions, which are the "true" sparse representation for 3D surfaces. In this paper, the non-subsampled shearlet transform (NSST) proposed by Easley et al. [20] is applied to analyze engineering surfaces. NSST combines the non-subsampled pyramid transform with several different shearing filters, which satisfies the property of shift invariance. Lacking of shift invariance means that small shifts in the input signals can induce major variations in the distribution of energy between wavelet coefficients at different scales. NSST possesses several nice properties including fully shift-invariance, multi-scale, and multi-direction, which make it a powerful tool in the analysis of 3D surfaces. It is worth noting that although shearlets have been used in image fusion [21], image denoising [20] and image classification [22], there is little effort made on the applications of using shearlets to filter and characterize 3D engineering surfaces.

The rest part of this paper is organized as follows: the theory of shearlets is described in Section 2. In Section 3, the proposed method of filtering 3D surface profiles with NSST is introduced. Also in this section, the transmission characteristics of NSST are analyzed. In Section 4, a simulation experiment is conducted to validate the feasibility of the presented method. Section 5 presents three case studies using different kinds of engineering surfaces to show the effectiveness of the proposed method in practical application. Section 6 draws conclusions of this work.

2. The construction of shearlets

The shearlet transform is built on the theory of composite wavelets, which is introduced in [19,20] and provides an effective approach for combining geometry and multi-scale analysis by utilizing the classical theory of affine systems. In two dimensions, the affine systems with composite dilations are defined as follows:

$$\{\psi_{j,l,k}(x)\} = \{|\det A|^{j/2}\psi(B^l A^j x - k) : j, l \in Z, k \in Z^2\} \quad (1)$$

where $\psi \in L^2(R^2)$ ($L^2(R^2)$ is the two-dimensional Hilbert space) and denotes the basic function, the anisotropic dilation matrix A and the direction matrix B are both 2×2 invertible matrices and $|\det B|=1$. j, l, k are scale, direction and shift parameter respectively and x denotes the input signal, Z denotes the set of all integers.

If $\psi_{j,l,k}(x)$ forms a Parseval frame for $L^2(R^2)$, then the elements of this system are called composite wavelets. The dilation matrices A^j refer to scale transformations, while the matrices B^l refer to geometrical transformations, such as rotations and shear. Shearlets are a special example of composite wavelets in $L^2(R^2)$, where $A = A_0$ is the anisotropic dilation matrix and $B = B_0$ is the shear matrix, which are given by

$$A_0 = \begin{pmatrix} 4 & 0 \\ 0 & 2 \end{pmatrix}, \quad B_0 = \begin{pmatrix} 1 & 1 \\ 0 & 1 \end{pmatrix} \quad (2)$$

For any $\xi = (\xi_1, \xi_2) \in \hat{R}^2$, $\xi_1 \neq 0$, let

$$\hat{\psi}^{(0)}(\xi) = \hat{\psi}^{(0)}(\xi_1, \xi_2) = \hat{\psi}_1(\xi_1)\hat{\psi}_2\left(\frac{\xi_2}{\xi_1}\right) \quad (3)$$

where $\hat{\psi}_1$, $\hat{\psi}_2$ are the Fourier transforms of ψ_1, ψ_2 respectively and $\hat{\psi}_1, \hat{\psi}_2 \in C^\infty(\hat{R})$, $\operatorname{supp}\hat{\psi}_1 \subset [-(1/2), -(1/16)] \cup [(1/16), (1/2)]$ and $\operatorname{supp}\hat{\psi}_2 \subset [-1, 1]$ ("supp" denotes support region).

Eq. (3) denotes that $\hat{\psi}^{(0)}$ is a compactly supported C^∞ function with support in $[-(1/2), (1/2)]^2$. In addition, assuming that

$$\sum_{j\geq 0} |\hat{\psi}_1(2^{-2j}\omega)|^2 = 1 \quad \text{for } |\omega| \geq \frac{1}{8} \quad (4)$$

And, for each $j \geq 0$,

$$\sum_{l=-2^j}^{2^j-1} |\hat{\psi}_2(2^j\omega - l)|^2 = 1 \quad \text{for } |\omega| \leq 1 \quad (5)$$

The conditions on the support of $\hat{\psi}_1$ and $\hat{\psi}_2$ imply that the functions $\hat{\psi}_{j,l,k}$ have frequency support:

$$\operatorname{Supp}\hat{\psi}_{j,l,k} \subset \left\{(\xi_1, \xi_2) : \xi_1 \in [-2^{2j-1}, -2^{2j-4}] \cup [2^{2j-4}, 2^{2j-1}], \left|\frac{\xi_2}{\xi_1} + l2^{-j}\right| \leq 2^{-j}\right\} \quad (6)$$

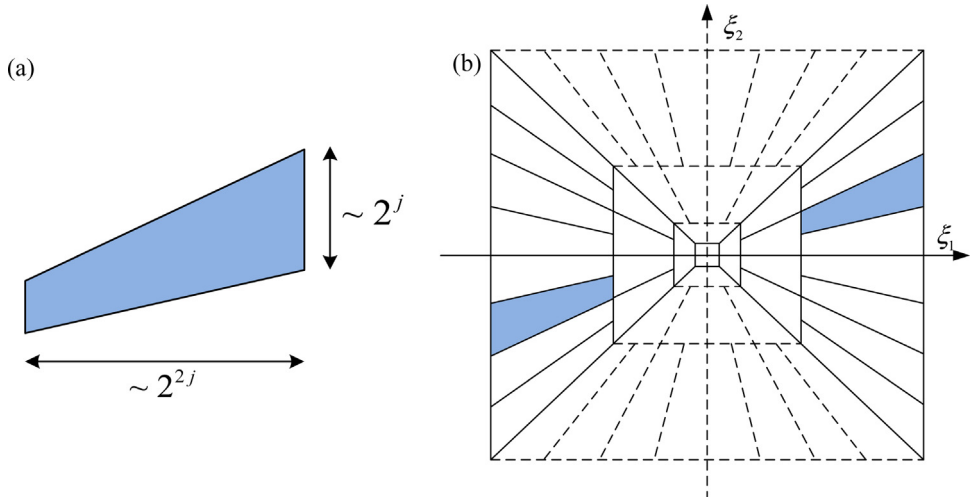

Fig. 1. (a) The frequency support of a shearlet (b) the tiling of the frequency plane induced by shearlets.

Thus, each element $\hat{\psi}_{j,l,k}$ is supported on a pair of trapezoids, contained in a box of approximate size $2^{2j} \times 2^j$, oriented along lines of slope $l2^{-j}$ (as shown in Fig. 1(a)).

From Eqs. (4) and (5), it follows that

$$\sum_{j\geq 0}\sum_{l=-2^j}^{2^j-1} |\hat{\psi}^{(0)}(\xi A_0^{-j} B_0^{-l})|^2 = \sum_{j\geq 0}\sum_{l=-2^j}^{2^j-1} |\hat{\psi}_1(2^{-2j}\xi_1)|^2 \left|\hat{\psi}_2\left(2^j \frac{\xi_2}{\xi_1} - l\right)\right|^2 = 1 \tag{7}$$

for $(\xi_1, \xi_2) \in D_0$, where D_0 is the horizontal cone: $D_0 = \{(\xi_1, \xi_2) \in \hat{R}^2 : |\xi_1| \geq (1/8), |(\xi_2/\xi_1)| \leq 1\}$. This means that the functions $\hat{\psi}^{(0)}(\xi A_0^{-j} B_0^{-l})$ form a tiling of D_0, which is demonstrated in Fig. 1(b) (the tiling of D_0 is illustrated in solid line while the tiling of D_1 in dashed line). This property, together with the fact that $\hat{\psi}^{(0)}$ is supported in $[-(1/2), (1/2)]^2$, denotes that the collection defined by

$$\{\psi^{(0)}_{j,l,k}(x) = 2^{3j/2}\psi^{(0)}(B_0^l A_0^j x - k) : j \geq 0, -2^j \leq l \leq 2^j - 1, k \in Z^2\} \tag{8}$$

is a Parseval frame for $L^2(D_0)^\vee = \{f \in L^2(R^2) : supp\hat{f} \subset D_0\}$.

Similarly, a Parseval frame can be constructed for $L^2(D_1)^\vee$, where D_1 is the vertical cone: $D_1 = \{(\xi_1, \xi_2) \in \hat{R}^2 : |\xi_2| \geq (1/8), |(\xi_1/\xi_2)| \leq 1\}$. Let

$$A_1 = \begin{pmatrix} 2 & 0 \\ 0 & 4 \end{pmatrix}, \quad B_1 = \begin{pmatrix} 1 & 0 \\ 1 & 1 \end{pmatrix} \tag{9}$$

and $\psi^{(1)}$ be given by

$$\hat{\psi}^{(1)}(\xi) = \hat{\psi}^{(1)}(\xi_1, \xi_2) = \hat{\psi}_1(\xi_2)\hat{\psi}_2\left(\frac{\xi_1}{\xi_2}\right) \tag{10}$$

where $\hat{\psi}_1$, $\hat{\psi}_2$ are defined as above. Then the collection defined by

$$\{\psi^{(1)}_{j,l,k}(x) = 2^{3j/2}\psi^{(1)}(B_1^l A_1^j x - k) : j \geq 0, -2^j \leq l \leq 2^j - 1, k \in Z^2\} \tag{11}$$

is a Parseval frame for $L^2(D_1)^\vee$.

Finally, let $\hat{\varphi} \in C_0^\infty(R^2)$ be chosen to satisfy

$$G(\xi) = |\hat{\varphi}(\xi)|^2 + \sum_{j\geq 0}\sum_{l=-2^j}^{2^j-1} |\hat{\psi}^{(0)}(\xi A_0^{-j} B_0^{-l})|^2 \chi_{D_0}(\xi) + \sum_{j\geq 0}\sum_{l=-2^j}^{2^j-1} |\hat{\psi}^{(1)}(\xi A_0^{-j} B_0^{-l})|^2 \chi_{D_1}(\xi) = 1, \quad \text{for } \xi \in \hat{R}^2 \tag{12}$$

where χ_D is the indicator function of the set D. This denotes that the support of $\hat{\varphi}$ is contained in $[-(1/8), (1/8)]^2$, with $|\hat{\varphi}(\xi)| = 1$ for $\xi \in [-(1/16), (1/16)]^2$, and the set $\{\varphi_k(x) : k \in Z^2\}$, defined by $\varphi_k(x) = \varphi(x - k)$, is a Parseval frame. Thus, we have the following result:

Theorem 1. Let $\varphi_k(x) = \varphi(x - k)$ and $\psi^{(d)}_{j,l,k}(x) = 2^{3j/2}\psi^{(d)}(B_d^l A_d^j x - k)$, where φ, ψ are given as above, then the collection of shearlets:

$$\{\varphi_k(x) : k \in Z^2\} \cup \{\psi^{(d)}_{j,l,k}(x) : j \geq 0, -2^j + 1 \leq l \leq 2^j - 2, k \in Z^2, d = 0, 1\} \cup \{\tilde{\psi}^{(d)}_{j,l,k}(x) : j \geq 0, l = -2^j, 2^j - 1, k \in Z^2, d = 0, 1\} \tag{13}$$

is a Parseval frame for $L^2(R^2)$, where $\hat{\tilde{\psi}}^{(d)}_{j,l,k}(\xi) = \hat{\psi}^{(d)}_{j,l,k}(\xi)\chi_{D_d}(\xi)$.

For $d = 0, 1$, the shearlet transform is mapping $f \in L^2(R^2)$ into the elements $\langle f, \psi^{(d)}_{j,l,k}\rangle$, where $j \geq 0, -2^j \leq l \leq 2^j - 1, k \in Z^2$.

3. The procedure of the proposed 3D surface separation method

3.1. Overview of the proposed method

This section provides an overview with respect to the separation of engineering surfaces. The developed method consists of two modules—decomposition of the original surface with NSST and reconstruction of the three surface components (form, waviness, roughness) with Inverse NSST. In Module 1, a L-level decomposition is conducted on the original surface to obtain coefficients of shearlet sub-bands in different directions and scales, and these shearlet coefficients in turn contain the texture information of the original surface at different scales with different directions. In Module 2, surface components at different levels are reconstructed by implementing an inverse NSST on the shearlet coefficients and combined into three surface components based on the cut-off wavelengths.

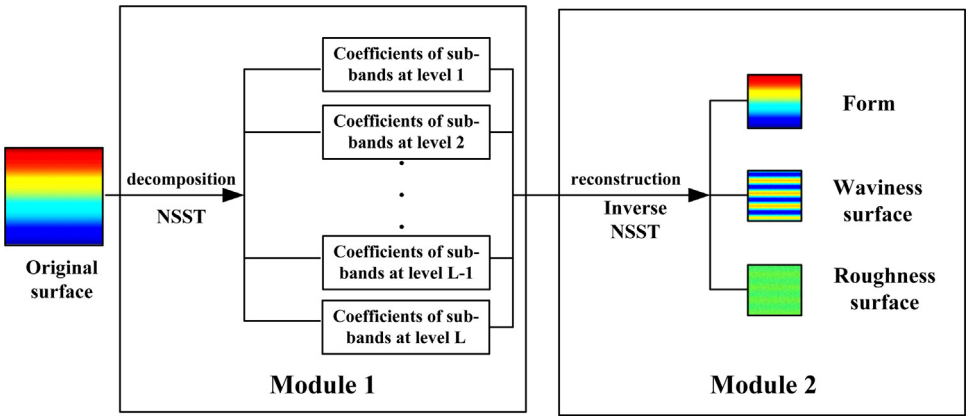

Fig. 2. The architecture of the proposed 3D surface separation method.

The procedure of Module 1 is described in details in Section 3.2 while the procedure of Module 2 is elaborated in Section 3.3 (Fig. 2).

3.2. The procedure of surface decomposition with NSST

The discrete shift-invariant shearlet transform can be implemented by two steps: multi-scale separation and directional localization. Alien from the standard shearlet transform, the multi-scale separation of shift-invariant shearlet transform is implemented by non-subsampled pyramid filter scheme that is efficient to add shift-invariance to the standard shearlet transform. This also explains why the shift-invariant shearlet transform is called non-subsampled shearlet transform (NSST). The procedure of NSST described above can be summarized as follows:

(1) Initialization: $j = L$ (L is the decomposition level); f is the input image;
(2) By applying non-subsampled Laplacian Pyramid filter (maximally flat filters are adopted as pyramid filter), the original image f is decomposed into a low-pass filtered image f_a^j (image of approximations at level j) and a high-pass filtered image f_d^j (image of details at level j);
(3) $\hat{f}_d^j$ is calculated on a pseudo-polar grid, and a matrix Pf_d^j is generated;
(4) The matrix Pf_d^j is processed by a band-pass filtering;
(5) The Cartesian sampled values are re-assembled directly, and then the inverse two-dimensional FFT (Fast Fourier Transform) is calculated. Then, the coefficients of shearlets at level j are obtained.
(6) $j = j - 1$, repeat steps (2)–(6) until $j = 1$.

In the above procedure, the function of step (2) is to decompose the two-dimensional signals into components of different scales, and the role of step (3)–(5) is to obtain the sub-bands of different orientations. To illustrate this procedure, a three-level decomposition using NSST is presented in Fig. 3. Here a_1^C is the low-frequency shearlet coefficient while $d_j^C (j = 1, 2, \ldots, L)$ are the high-frequency shearlet coefficients. Since directional filtering is implemented on detail image at each level, the expression of d_j^C is obtained as follows:

$$d_j^C = (d_j^1, d_j^2, \ldots, d_j^{n_j}), j = 1, 2, \ldots, L \tag{14}$$

where n_j is the number of directions at level j. As j increases, the texture information contained in the high-frequency shearlet coefficients at level j becomes finer and finer.

Fig. 4 illustrates a two-level decomposition of the "Zoneplate" image using non-subsample shearlet transform. The direction vector is $\vec{n} = (n_1, n_2) = (4, 6)$. The first level decomposition generates four directional sub-bands, and the second level decomposition generates six directional sub-bands. It should be noted that the

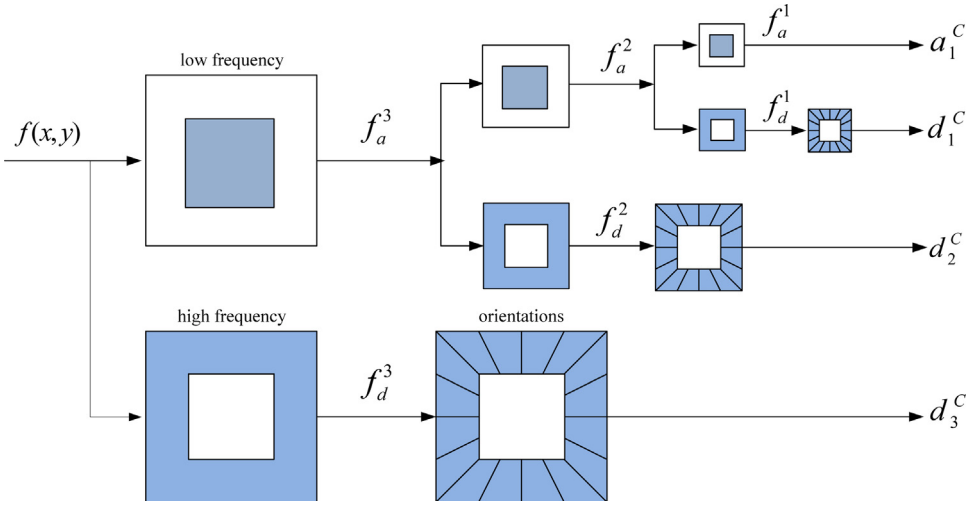

Fig. 3. A three-level decomposition using NSST.

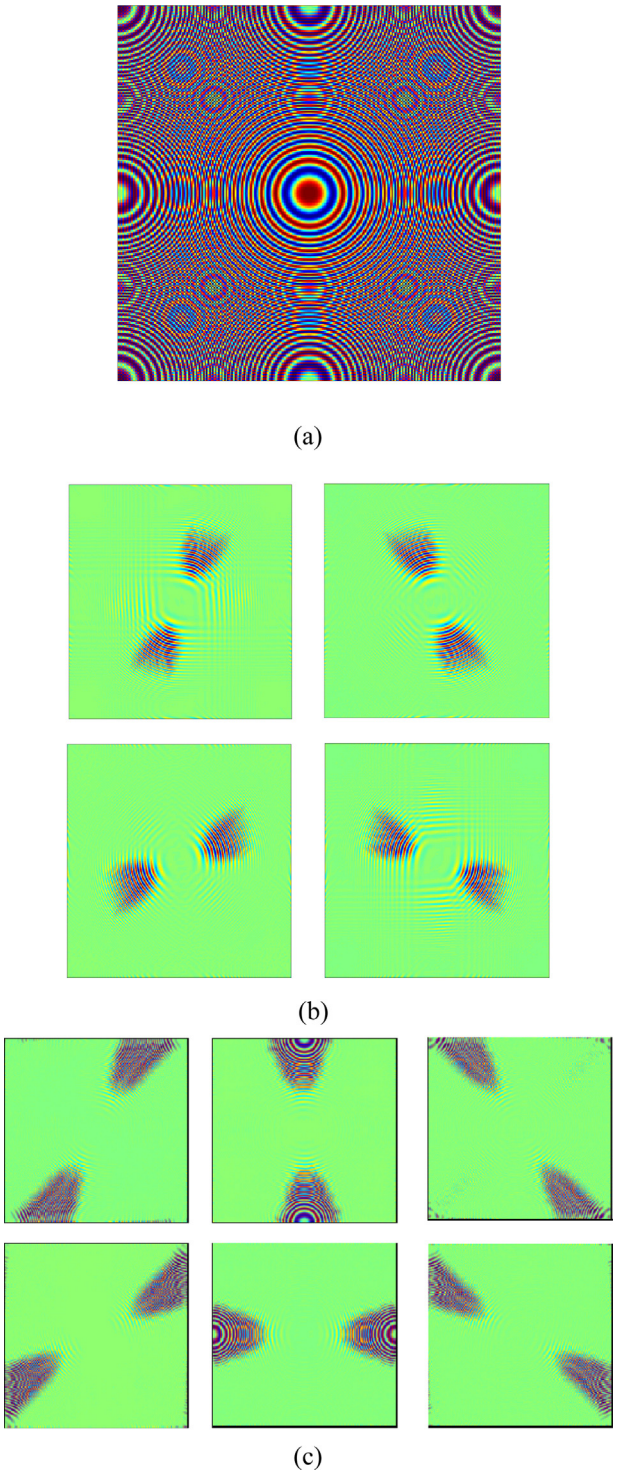

Fig. 4. (a) The "Zoneplate" image (b) coefficients of four directions at the first level and (c) coefficients of six directions at the second level.

directions of sub-bands are not fixed at each level, and a variety of directions can be obtained through shearlet transform.

3.3. The procedure of surface reconstruction with INSST

Engineering surfaces are regarded as having fine texture called roughness, superimposed on more general curvature called waviness, and long range deviations called form. In this way, an engineering surface $S(x, y)$ can be separated as follows:

$$S(x, y) = R(x, y) + W(x, y) + F(x, y) \tag{15}$$

where $R(x, y)$ represents the roughness components, $W(x, y)$ represents the waviness components, and $F(x, y)$ represents the form components.

These surface components can be separated in the multi-scale domain by shearlets. The high-frequency shearlet coefficients at the finest levels (highest levels) can be deemed as the outputs of a high-pass filter band ($1/\lambda_0 \sim 1/\lambda_{rc}$) and refer to the roughness components $R(x, y)$. Here λ_0 denotes the sampling interval, λ_{rc} denotes the cut-off wavelength of the roughness. The high-frequency shearlet coefficients at the medium levels can be deemed as the outputs of the sub-low pass filter band ($1/\lambda_{rc} \sim 1/\lambda_{wc}$) and refer to the waviness components $W(x, y)$. Here λ_{wc} refer to the cut-off wavelength of the waviness. Likewise, the low-frequency shearlet coefficients at the coarsest level (lowest level) can be considered as the outputs of the low-pass filter band ($1/\lambda_{wc} \sim 1/\lambda_l$). Here λ_l denotes the sampling length. Based on an inverse non-subsampled shearlet transform (INSST), these surface components can be reconstructed respectively:

$$\begin{cases} \text{Form} : F(x, y) = \text{INSST}(a_1^C) \\ \text{Waviness} : W(x, y) = \text{INSST}(d_{j_w}^C, \ldots, d_{j_r}^C) \\ \text{Roughness} : R(x, y) = \text{INSST}(d_{j_r}^C, \ldots, d_L^C) \end{cases} \tag{16}$$

where a_1^C are the shearlet coefficients of the low-pass sub-bands, $d_j^C (j = 1, \ldots, L)$ are the shearlet coefficients of the high-pass sub-bands, j_r is the level in which the cut-off wavelength of the roughness locates, and j_w is the level in which the cut-off wavelength of the waviness locates (usually $j_w = 1$).

Then the cut-off wavelengths of roughness and waviness by shearlets can be obtained as follows:

$$\lambda_{rc} = \lambda_0 \times 2^{(3/2)(L-j_r+1)} \tag{17}$$

$$\lambda_{wc} = \lambda_0 \times 2^{(3/2)(L-j_w+1)} \tag{18}$$

To show the reconstruction performance of shearlets, Fig. 5 presents the components of the reconstructed images of a light circular disc on a dark background (see Fig. 5(a)), for reconstructed images of high-frequency sub-bands (details) at levels 1–3 and low-frequency sub-bands (approximations) at level 1, using NSST, 2D DWT (Antonini 9-7 tap filters are used as mother wavelets) and 2D DT-CWT (Near-Symmetric 13, 19 tap filters are used for level 1 and Q-Shift 14, 14 tap filters for other levels) respectively. In Fig. 5(c), it can be seen that irregular edges and stripes are almost normal to the edge of the disc in places. The reconstructed images in Fig. 5(d) are better than those of Fig. 5(c), since the artifacts showed in Fig. 5(d) are almost absent here. However, In contrast with DWT and DT-CWT, NSST performs best in reconstruction of the disc images, due to the fact that the reconstructed images are smooth, continuous and clear. The images in Fig. 5(b) demonstrate good shift invariance because all parts of the disc edge are treated equivalently. Moreover, these images also show good rotational invariance, since each reconstructed image is using coefficients from all the different directional sub-bands at a given level.

3.4. Transmission characteristics of shearlet filter

To separate different surface components properly, a wavelet filtering method needs to satisfy three properties: (1) Finite Impulse Response (FIR), guarantees that the supporting length of filter's weighting function is finite, (2) zero or linear phase, ensures that there will be no distortion in the filtered profiles, and (3) shape amplitude transmission, ensures that a low-pass filter transmits almost all the wavelengths above a certain cut-off without attenuating its amplitude and heavily suppresses wavelengths below

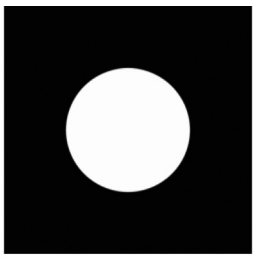

(a) The 'disc' image

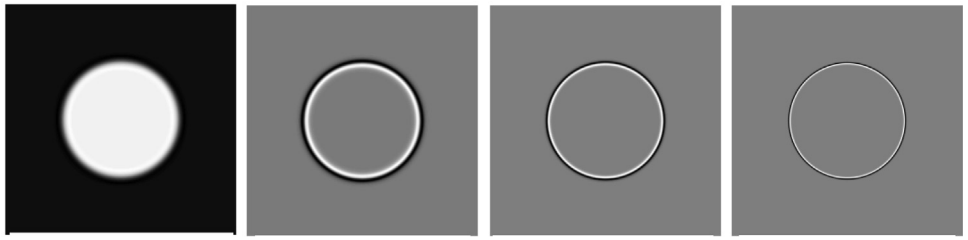

(b) NSST

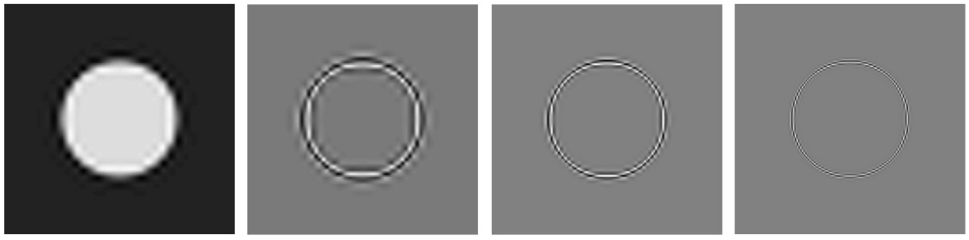

(c) DWT

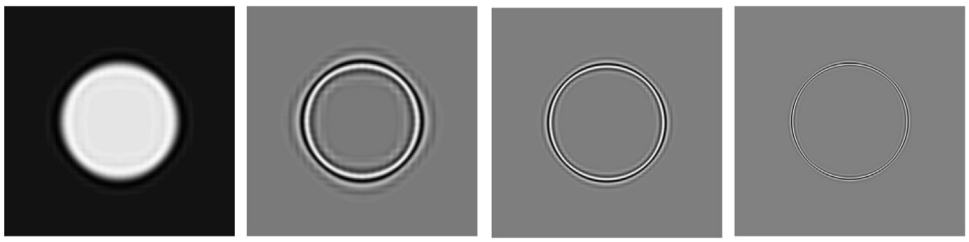

(d) DT-CWT

Fig. 5. (a) The 'disc' image (b) reconstructed images at 3 levels using NSST (c) reconstructed images at 3 levels using 2D DWT (d) reconstructed images at 3 levels using 2D DT-CWT.

the cut-off and vice versa for the high-pass filter. The transmission characteristics of shearlet filter will be discussed in the following part.

3.4.1. Phase transmission characteristics

A filter that produces different phase offsets for different input wavelengths is not desirable since the filtered output will have distortions. To overcome this problem, a filter needs to have zero or linear phase. Since FIR filters corresponding to tight frames cannot be linear-phase except for Haar-type filters, which denotes that linear phase filters and tight frames are mutually exclusive. The pseudo-inverse is desirable, but is Infinite Impulse Response (IIR) if the frame is not tight [23]. Consequently, an FIR Non-subsampled Filter Bank (NSFB) system with linear phase filters and with synthesis filters corresponding to the pseudo inverse is not possible. However, the pseudo-inverse can be approximated with FIR filters. In this study, the maximally flat filters are used as 2D pyramid filter in the procedure of NSST. The design of maximally flat filters is discussed in details in [24]. Maximally flat filters are zero-phase filters that under a frame which is very close to a tight one, which means that shearlet filter has zero-phase transmission characteristics.

3.4.2. Amplitude transmission characteristics

Fig. 6 presents the amplitude transmission characteristics of Gaussian filter and shearlet filter. The cut-off wavelengths in x and y directions are both set to 0.64 mm, λx and λy denote the

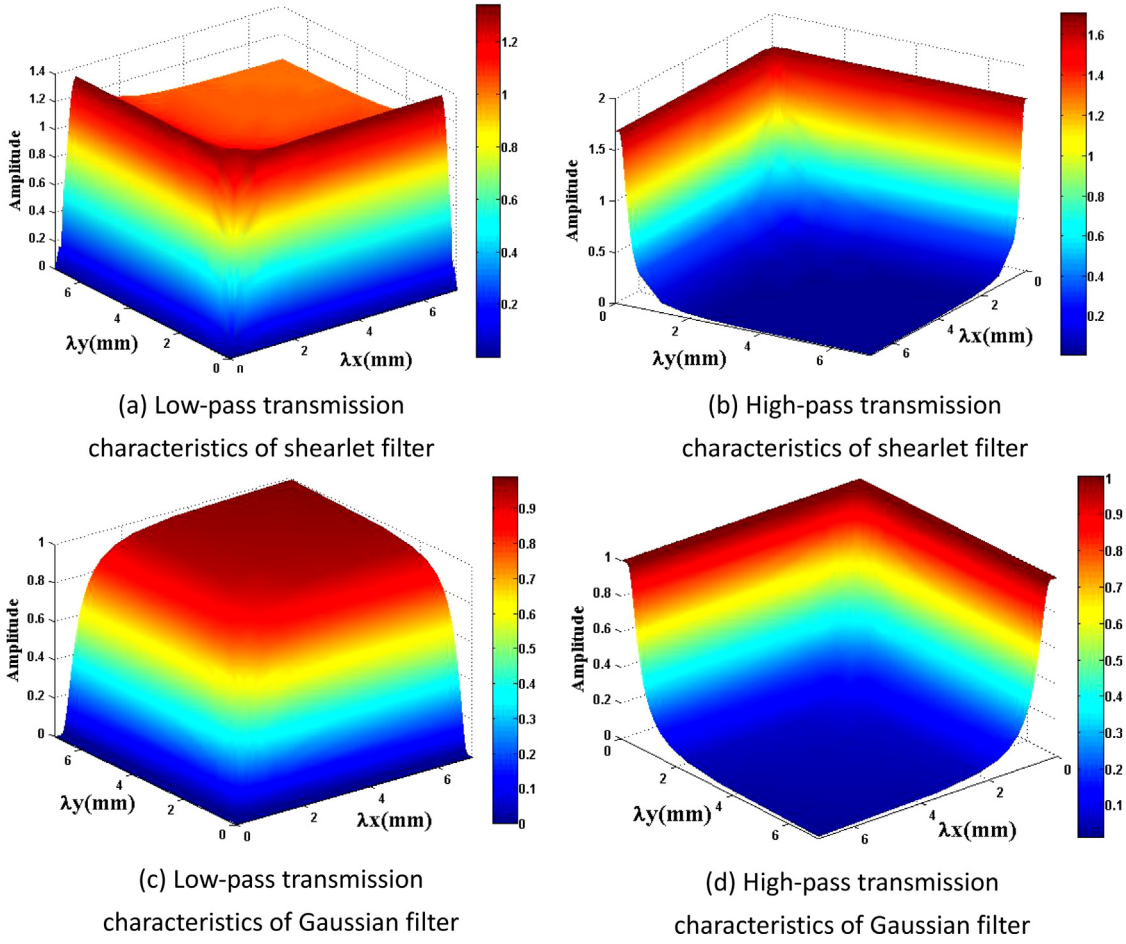

Fig. 6. Transmission characteristics of shearlet filter and Gaussian filter.

wavelength in x-axis and y-axis respectively. It is well known that a desirable 2D filtering method should have a steep amplitude transmission curve near the cut-off wavelength. Likewise, a steeper amplitude transmission profile is preferred in the filtering of 3D surfaces. It can be seen from Fig. 6 that both the low-pass and high-pass amplitude transmission profile of shearlet filter near the cut-off wavelengths are steeper than those of Gaussian filter, which demonstrates that shearlet filter can separate out different frequency surface components effectively.

4. Numerical simulation

To verify the performance of NSST, a simulated surface (as shown in Fig. 7(a)) is generated and filtered using the proposed method. The size of the simulated surface is 40 mm × 40 mm, the sampling interval is 0.1 mm, and the numerical expression of the surface is as follows:

$$z(x, y) = 0.002x + 0.002\sin(0.2\pi x) + 0.001\,\text{normrnd}(0, 0.1),$$
$$0 \le x \le 40\,\text{mm}, 0 \le y \le 40\,\text{mm} \quad (19)$$

where normrnd(μ, δ) denotes random number subjects to the normal distribution with mean parameter μ and standard deviation parameter δ.

The first item on the right side of Eq. (19) can be deemed as the form components (an inclined surface), the second item is a sinusoidal function that can be deemed as the waviness components, and the third item are the random noises added to the surface, which can be deemed as the roughness components. Then the NSST is applied to decompose the simulated surface into high-frequency details and low-resolution approximations of five levels. If the two highest levels of details are combined as roughness ($j_r = 4$) and the three lowest levels of details are combined as the waviness ($j_w = 1$), Fig. 7(c) and (d) are obtained. In this way, the cut-off wavelength of the roughness λ_{rc} is $0.1 \times (2^{3/2})^2 = 0.8$ mm, the cut-off wavelength of the waviness λ_{wc} is $0.1 \times (2^{3/2})^5 = 18.1$ mm. The lowest level of the approximation is considered as the form shown in Fig. 7(b). It can be found from Fig. 7 that the proposed method is feasible since different surface components are separated properly by shearlets.

5. Case studies

5.1. Case Study I

Engineering surfaces, which are presented by point cloud data collected by a device called Coherix ShaPix [25], are used to demonstrate the effectiveness of the proposed method for surface texture analysis in practical applications. ShaPix is a novel laser holographic interferometer which uses a tunable-wavelength laser to gather up to 1 million data points about the part in its micron level. This high definition metrology (HDM) provides a good platform to develop new surface analysis methods that involving surface texture separation and surface feature characterization. In the last few years, some efforts have been made to use it to analyze engineering surfaces [16,26]. A large number of high-resolution data of engineering surfaces can be obtained by this device, which is served as the input of filtering. All the HDM data of engineering surfaces in case studies

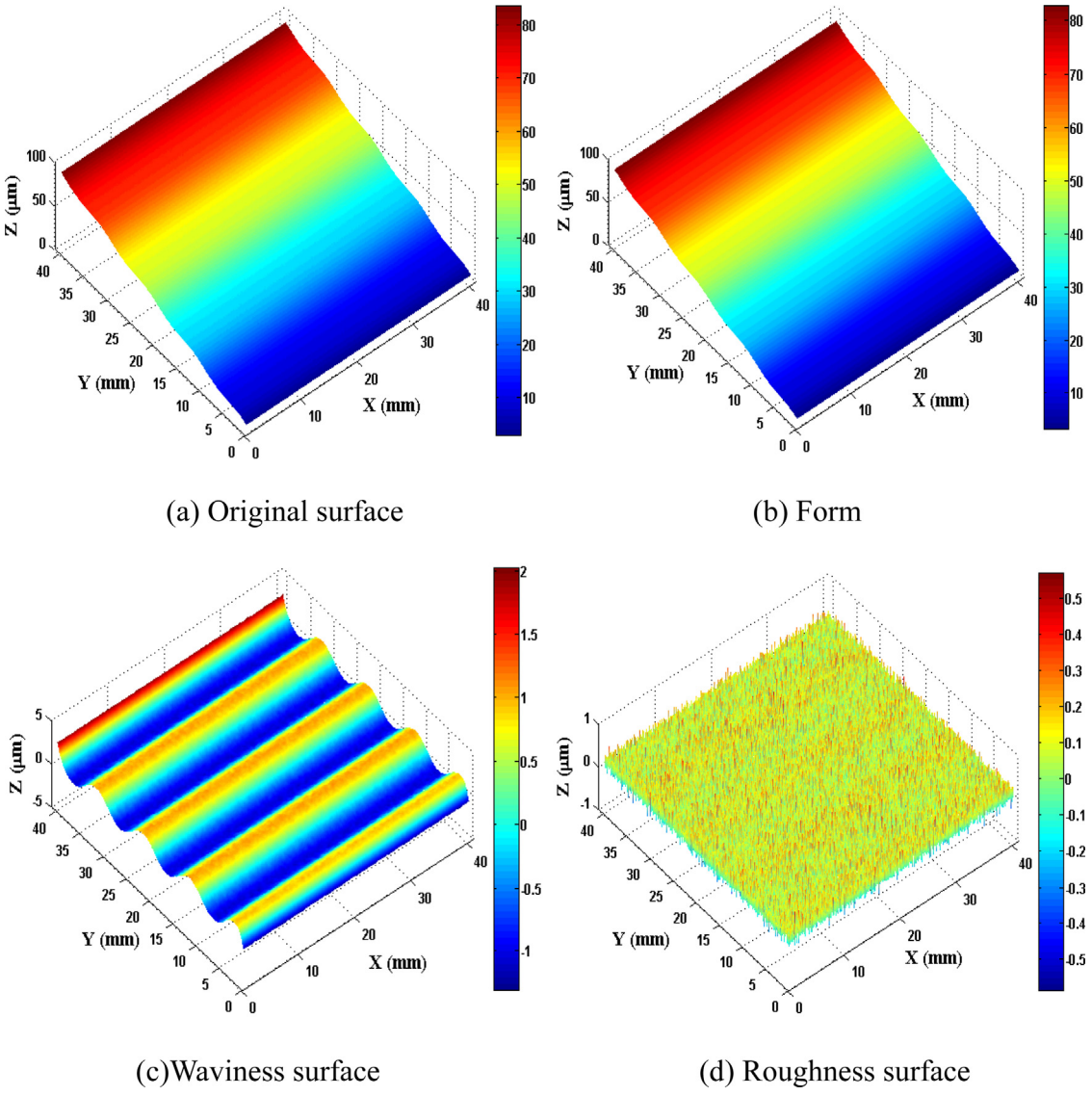

Fig. 7. Surface texture decomposition with shearlet filter.

are measured by Shapix and the engineering surface in this subsection is the top surface of an engine cylinder block (as shown in Fig. 8) processed by a major domestic car manufacturer. The material of the engine cylinder block is Cast iron FC250. This top surface is produced by milling. The milling process was carried out on an EX-CELL-O machining center using a milling cutter with a diameter of 200 mm. The milling speed was 816.4 m/min, the depth of milling was 0.5 mm, and feed rate was 3360 mm/min. The 3D height map of this surface is shown in Fig. 9. The units of x-axis, y-axis and height are mm.

A small piece of surface is randomly selected from the top surface, as shown in Fig. 10(a), the size of the selected surface is 6.4 mm × 6.4 mm and the sampling interval is 0.01 mm. Then an eight-level decomposition is implemented on the surface data using NSST.

If the reconstruction is applied by combining the four highest levels (levels 5–8) of details as roughness ($j_r = 5$), the four lowest levels of details (levels 1–4) as waviness ($j_w = 1$) and approximations at level 1 as form, the results can be obtained as shown in Fig. 10.

For the purpose of comparing the proposed method with the current standard filtering technique, the International

Fig. 8. The top surface of an engine cylinder block.

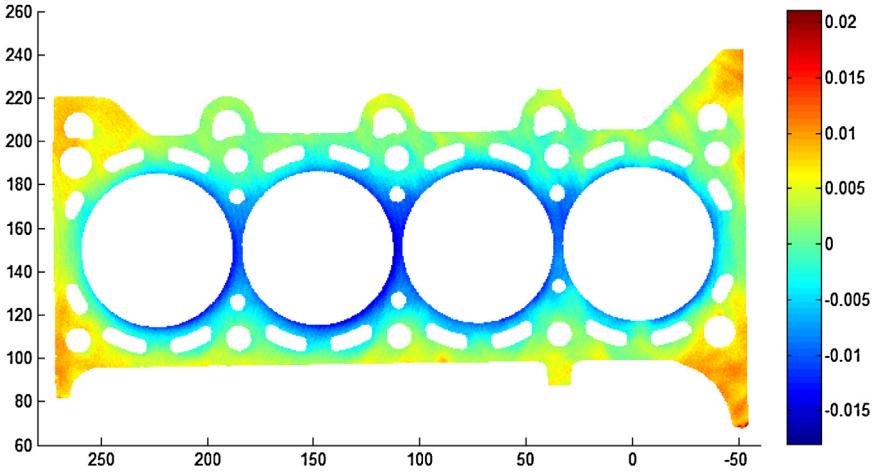

Fig. 9. The 3D height map of the top surface.

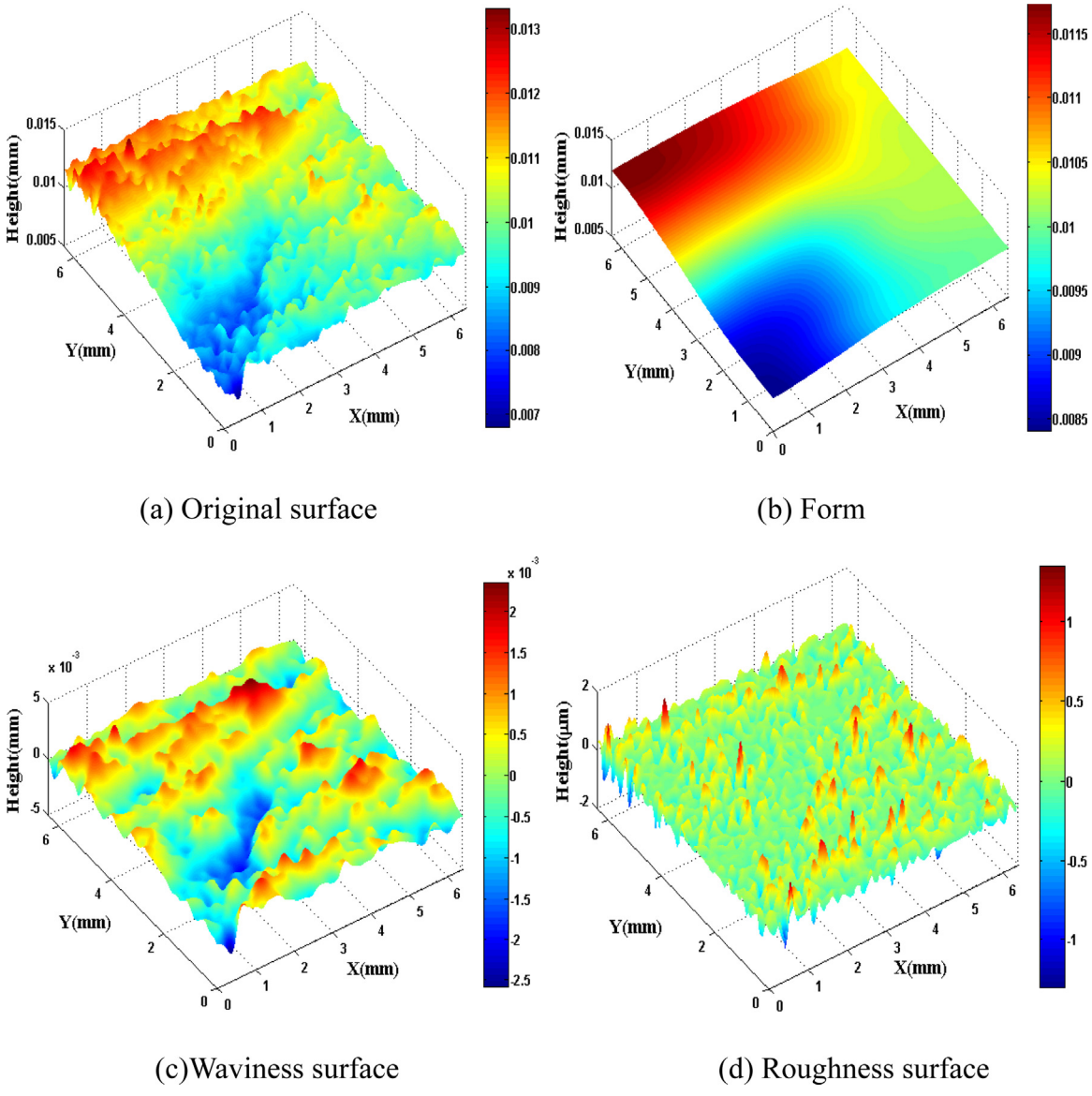

Fig. 10. Surface texture decomposition with shearlet filter.

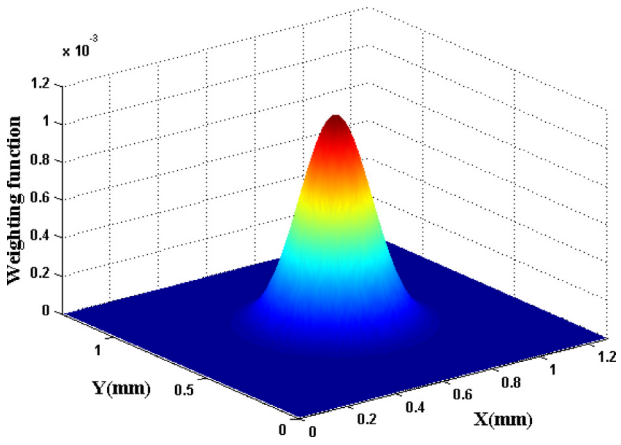

Fig. 11. Weighting function of 3D Gaussian filter.

Organization for Standardization (ISO) Gaussian filter is implemented. The weighing function of the 3D Gaussian filter is a simple 3D extension of the 2D Gaussian filter:

$$S(x,y)=\frac{1}{\alpha^2\lambda_{xc}\lambda_{yc}}\exp\left[-\left[\pi\left(\frac{x}{\alpha\lambda_{xc}}\right)^2+\pi\left(\frac{y}{\alpha\lambda_{yc}}\right)^2\right]\right] \tag{20}$$

where λ_{xc} and λ_{yc} are the cutoff wavelengths in the x and y directions, and $\alpha=\sqrt{\ln 2/\pi}=0.4697$. The Gaussian filter is implemented using 2D convolution, which is mathematically convoluting the 2D Gaussian weighting function to the 3D height map. To be consistent with shearlet filter, the cut-off wavelengths in x and y directions are both set to $\lambda_{xc}=\lambda_{yc}=0.01\times(2^{3/2})^4=0.64$ mm (this value is also close to 0.8 mm, which is a recommended value from the ASME B46.1 Standard [15]). Then the weighting function can be determined mathematically, which is shown in Fig. 11. However, it should be noticed that Gaussian filter is haunted by edge distortion, which arouses excessive distortion near the boundary of the measuring area. And this phenomenon is inevitable due to the fact that the convolution in Gaussian filter is performed on finite-size image. In this study, the first and last cut-off wavelengths are discarded after filtering in order to eliminate the edge effects and the actual size of the evaluation area is 5.12 mm × 5.12 mm. The surface data is separated into two components using Gaussian filter, one is the mean surface and the other is the roughness surface. They are shown in Fig. 12. It is noted that the mean surface actually is the combination of two surface components including waviness and form. Fig. 13 presents a comparison of mean surfaces obtained by Gaussian filter and shearlet filter without discarding any boundary region (the size of evaluation area is 6.4 mm × 6.4 mm). Fig. 13(a) shows that there are serious distortions on the boundary of the mean surface obtained by Gaussian filter, and the height values on the boundary are approaching zero on account of convolution operation implemented in Gaussian filter. In contrast, Fig. 13(b) shows that shearlet filter is free from boundary distortion and therefore does not need to discard any evaluation area.

To further study the correlation between the results of the two methods, some 3D surface texture parameters are calculated based on the roughness surfaces obtained by shearlet filter and Gaussian filter. These 3D surface texture parameters include amplitude parameters (S_a, S_q and S_t), shape parameters (S_{ku}, S_{sk}) and spacing parameters (S_{al}, S_{tr}), which are able to compare the two filtering methods in a comprehensive way.

(1) Amplitude parameters

The average roughness parameter S_a is defined as:

$$S_a=\frac{1}{A}\iint_A|z(x,y)|dxdy \tag{21}$$

where $z(x,y)$ is the height value of the surface and A is the definition area.

The root mean square roughness parameter S_q is defined as:

$$S_q=\sqrt{\frac{1}{A}\iint_A z^2(x,y)dxdy} \tag{22}$$

The maximum height of texture surface S_t is defined as:

$$S_t=|\max(z(x,y)|+|\min(z(x,y))| \tag{23}$$

(2) Shape parameters

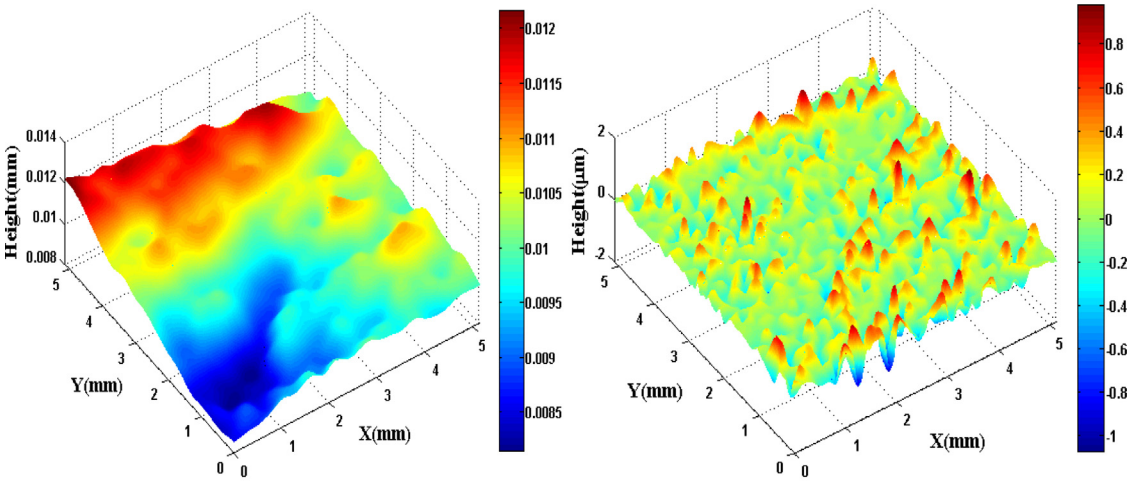

(a) Mean surface (b) Roughness surface

Fig. 12. Surface texture decomposition with Gaussian filter.

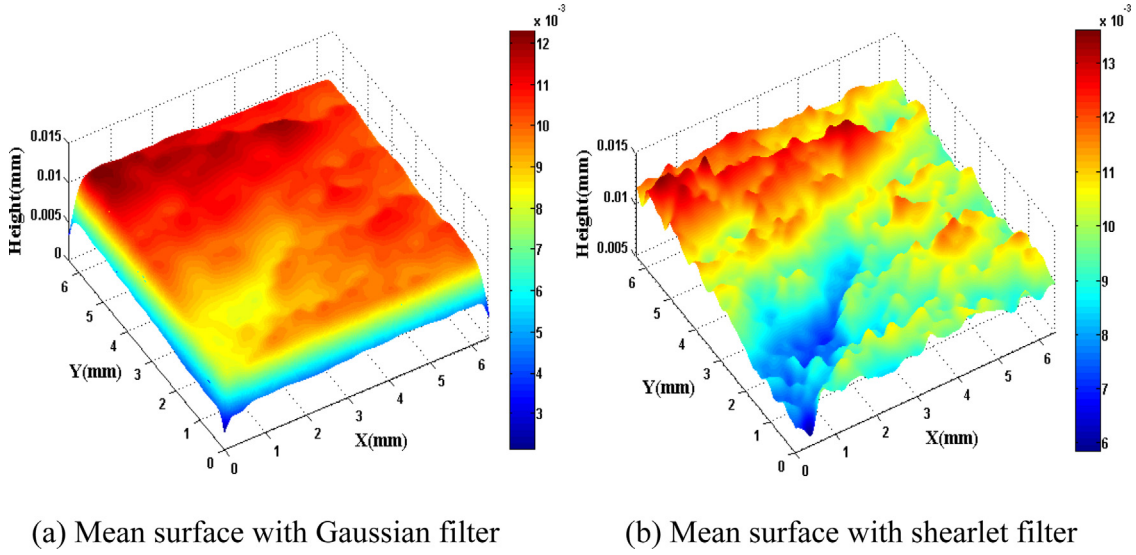

(a) Mean surface with Gaussian filter (b) Mean surface with shearlet filter

Fig. 13. Comparison of mean surfaces obtained by Gaussian filter and shearlet filter without discarding any boundary region.

The kurtosis of surface height distribution parameter S_{ku} is defined as:

$$S_{ku} = \frac{1}{sq^4}\left[\frac{1}{A}\iint_A z^4(x,y)dxdy\right] \tag{24}$$

The skewness of surface height distribution parameter S_{sk} is defined as:

$$S_{sk} = \frac{1}{sq^3}\left[\frac{1}{A}\iint_A z^3(x,y)dxdy\right] \tag{25}$$

(3) Spacing parameters

The spacing parameter S_{al} is the horizontal distance of the autocorrelation function that has the fasted decay in any direction to a specified threshold value η, with $0 < \eta < 1$ ($\eta = 0.1$ in this study).

$$S_{al} = \min_{\tau_x,\tau_y\in R}\left(\sqrt{\tau_x^2+\tau_y^2}\right) \quad \text{where } R = \{(\tau_x,\tau_y) : \mathrm{ACF}(\tau_x,\tau_y) \le \eta\} \tag{26}$$

The autocorrelation function (ACF) of a 3D surface is defined as a convolution of the surface with itself, shifted by (τ_x, τ_y):

$$\mathrm{ACF}(\tau_x,\tau_y) = \frac{\iint_A z(x,y)z(x-\tau_x,y-\tau_y)dxdy}{\iint_A z(x,y)z(x,y)dxdy} \tag{27}$$

The surface texture aspect ratio parameter S_{tr} is defined as:

$$S_{tr} = \frac{\min_{\tau_x,\tau_y\in R}\left(\sqrt{\tau_x^2+\tau_y^2}\right)}{\max_{\tau_x,\tau_y\in R}\left(\sqrt{\tau_x^2+\tau_y^2}\right)} \quad \text{where } R = \{(\tau_x,\tau_y) : \mathrm{ACF}(\tau_x,\tau_y) \le \eta\} \tag{28}$$

Three top surfaces of engine blocks (A–C) are selected and eight locations (locations 1–8, as shown in Fig. 14) from each top surface are selected for comparing with the same size (6.4 mm × 6.4 mm). To be convenient for comparison, the actual evaluation area with shearlet filter is set to the size of that with Gaussian filter (5.12 mm × 5.12 mm). Fig. 15 shows the separated roughness surface using two methods on top surface A respectively. It is observed that the separated roughness between shearlet filter and Gaussian filter are matched quite well in most corresponding locations.

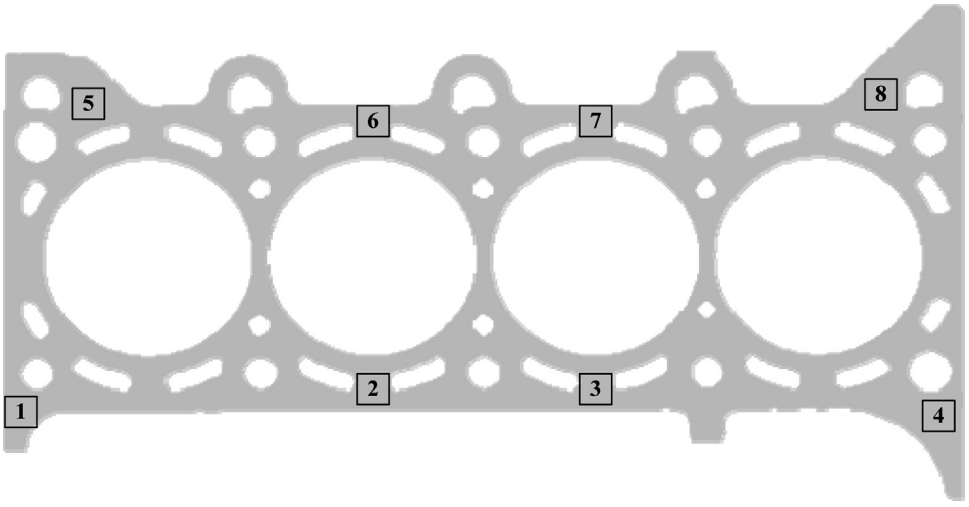

Fig. 14. Eight locations selected for comparison.

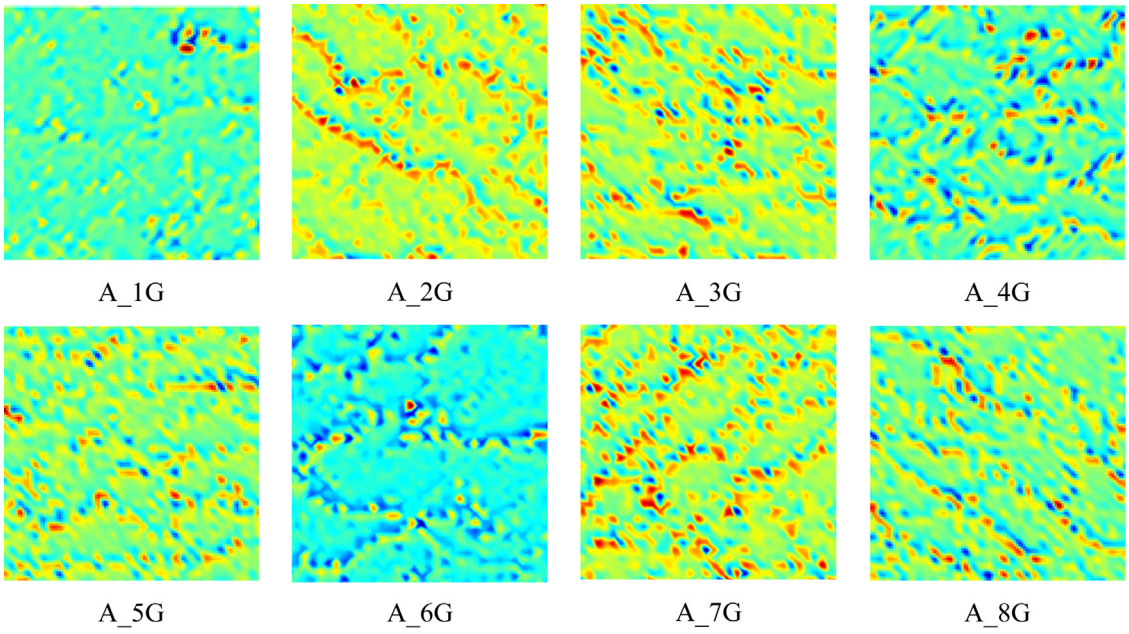

(a) Roughness surfaces with Gaussian filter

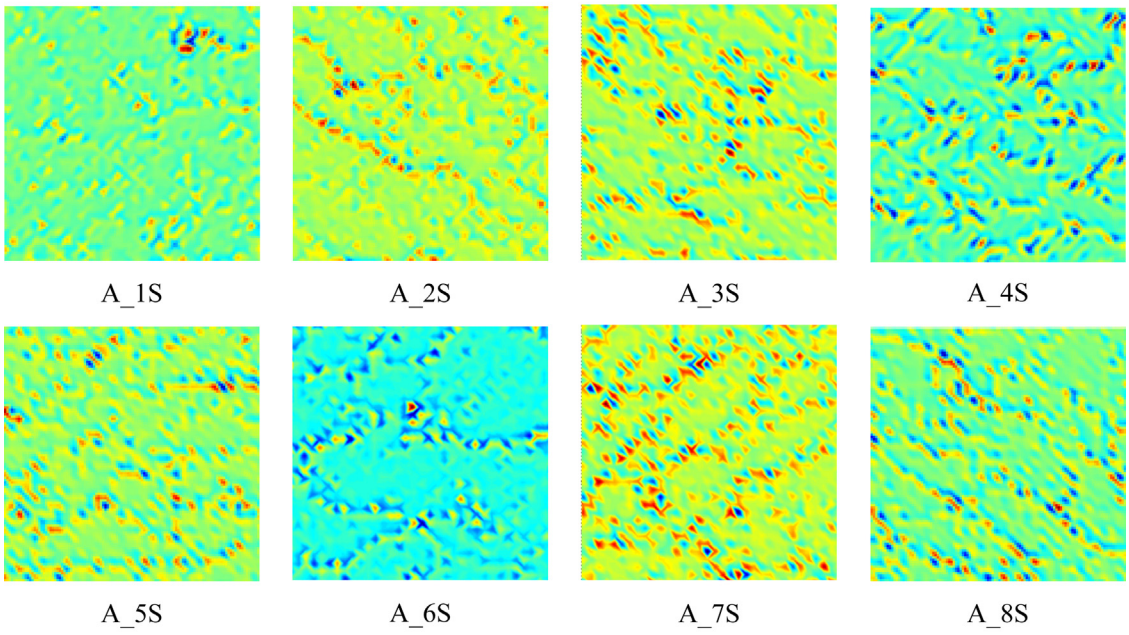

(b) Roughness surfaces with Shearlet filter

Fig. 15. The separated roughness surfaces using two methods respectively.

Tables 1 and 2 list all the surface texture parameters using these two methods and the differences between them. The differences in the surface texture parameters are due to the different transmission properties between shearlet filter and Gaussian filter. Nevertheless, it can be found from the last three columns in Table 1 that the differences are less than 5% in S_a values, less than 10% in S_q values and less than 20% in S_t values. It also can be found from the last four columns in Table 2 that the average differences of the shape and space parameters between the two methods are less than 25% in general. Since the variation of 10–20% or more in roughness parameters are very common as reported in [27] when using different filter banks, hence the comparison demonstrates that shearlet filter based parameters are correlated well with existing standards. However, it is worth noting that part of the evaluation area has to be discarded due to "edge effect" when using Gaussian filter, and now shearlet filter overcomes this problem without deviating from the standard values too much.

Since engine block top surface is only one of the many types of machined surfaces, other two different types of engineering surfaces are studied in this section to further validate the correlation between the two filtering methods.

5.2. Case Study II

The second engineering surface is the surface of a cylinder head which is made of aluminum. This surface is produced by milling.

Table 1
Comparison of amplitude parameters.

Unit: μm	Shearlet filter			Gaussian filter			Difference* (%)		
	S_a	S_q	S_t	S_a	S_q	S_t	S_a	S_q	S_t
A_1	0.117	0.171	2.981	0.116	0.165	2.694	1.298	3.695	10.648
A_2	0.117	0.168	2.661	0.122	0.167	2.128	3.692	0.179	25.038
A_3	0.141	0.198	2.449	0.140	0.189	2.066	0.930	4.873	18.518
A_4	0.140	0.195	2.111	0.140	0.190	1.879	0.286	2.630	12.337
A_5	0.164	0.226	2.828	0.160	0.214	2.457	2.313	5.844	15.104
A_6	0.126	0.188	2.861	0.128	0.183	2.404	1.098	3.063	19.014
A_7	0.147	0.205	2.236	0.143	0.193	1.905	2.722	6.276	17.354
A_8	0.146	0.204	2.279	0.143	0.194	1.983	2.311	5.271	14.912
A_avg.	0.137	0.194	2.551	0.136	0.187	2.190	1.831	3.979	16.616
B_1	0.145	0.207	2.486	0.145	0.199	2.049	0.275	3.962	21.359
B_2	0.143	0.205	3.049	0.143	0.199	2.583	0.279	2.708	18.026
B_3	0.146	0.202	2.084	0.147	0.196	1.777	0.409	2.857	17.234
B_4	0.152	0.213	2.825	0.156	0.211	2.206	2.184	1.138	28.055
B_5	0.162	0.230	3.097	0.162	0.222	2.731	0.370	3.785	13.402
B_6	0.153	0.211	2.965	0.153	0.204	2.372	0.261	3.234	24.968
B_7	0.165	0.229	2.509	0.167	0.221	2.145	1.197	3.300	16.956
B_8	0.159	0.220	2.577	0.156	0.209	2.270	1.408	5.065	13.500
B_avg.	0.153	0.215	2.699	0.154	0.208	2.267	0.798	3.256	19.187
C_1	0.151	0.223	3.431	0.147	0.210	2.919	2.239	6.140	17.542
C_2	0.129	0.182	2.456	0.130	0.176	2.121	0.309	3.643	15.776
C_3	0.133	0.191	2.884	0.131	0.179	2.244	1.606	6.522	28.498
C_4	0.137	0.195	2.716	0.137	0.189	2.362	0.073	3.183	14.968
C_5	0.137	0.196	2.695	0.137	0.187	2.216	0.073	4.541	21.600
C_6	0.130	0.188	2.357	0.129	0.178	1.940	0.620	5.624	21.490
C_7	0.143	0.202	2.578	0.146	0.198	2.220	1.784	1.816	16.127
C_8	0.154	0.218	2.899	0.148	0.203	2.350	4.062	7.185	23.371
C_avg.	0.139	0.199	2.752	0.138	0.190	2.297	1.346	4.832	19.922

* Difference is calculated as : $\left|\frac{\text{Shearlet value}-\text{Gaussian value}}{\text{Gaussian value}}\right| \times 100$.

The height map of this surface is shown in Fig. 16 and the units of x-axis, y-axis and height are mm. Eight locations are selected (locations 1–8, as shown in Fig. 17) from this surface with the same size and then eight small surfaces are obtained.

One of these selected surfaces (Location 1) is shown in Fig. 18. The size of evaluation area is 5.12 mm × 5.12 mm and the sampling interval is 0.01 mm. Then a six-level decomposition is implemented on this surface data using shearlet filter. If the reconstruction is

Table 2
Comparison of shape and space parameters.

	Shearlet filter				Gaussian filter				Difference (%)			
	S_{ku}	S_{sk}	S_{al}	S_{tr}	S_{ku}	S_{sk}	S_{al}	S_{tr}	S_{ku}	S_{sk}	S_{al}	S_{tr}
A_1	9.428	0.337	8.485	0.849	9.115	0.413	9.900	0.868	3.438	18.279	14.286	2.269
A_2	6.680	−0.165	8.544	0.854	5.025	−0.158	10.440	0.855	32.944	4.560	18.163	0.105
A_3	5.436	−0.269	7.616	0.595	4.525	−0.237	8.944	0.629	20.143	13.652	14.853	5.498
A_4	5.225	−0.054	8.944	0.970	4.538	−0.052	10.198	0.901	15.132	3.654	12.294	7.621
A_5	5.445	−0.183	7.616	0.633	4.581	−0.157	8.944	0.698	18.867	16.805	14.853	9.436
A_6	7.542	0.208	8.544	0.906	6.216	0.267	10.198	0.943	21.329	21.905	16.219	3.935
A_7	5.313	−0.064	7.616	0.668	4.375	−0.057	9.220	0.755	21.423	12.238	17.395	11.572
A_8	5.083	−0.103	7.071	0.552	4.441	−0.087	8.602	0.608	14.473	17.506	17.800	9.222
A_avg.	6.269	−0.037	8.055	0.753	5.352	−0.009	9.556	0.782	18.469	13.575	15.733	6.207
B_1	5.838	0.016	8.246	0.833	4.726	0.024	9.849	0.818	23.524	33.333	16.273	1.846
B_2	7.268	−0.270	8.544	0.906	6.204	−0.248	10.050	0.881	17.147	9.087	14.984	2.757
B_3	5.068	−0.155	7.616	0.595	4.251	−0.132	9.220	0.649	19.228	16.767	17.395	8.324
B_4	5.543	−0.037	8.944	0.948	4.415	−0.032	10.440	0.934	25.535	15.938	14.329	1.531
B_5	6.147	−0.157	7.616	0.595	5.036	−0.123	9.220	0.678	22.055	27.317	17.395	12.260
B_6	5.402	−0.057	8.485	0.899	4.264	−0.041	10.198	0.943	26.680	38.725	16.794	4.603
B_7	5.088	0.051	7.810	0.685	4.075	0.048	9.849	0.807	24.853	7.158	20.700	15.097
B_8	5.443	−0.119	7.071	0.552	4.538	−0.097	8.944	0.658	19.926	21.891	20.943	16.028
B_avg.	5.724	−0.091	8.042	0.752	4.689	−0.075	9.721	0.796	22.368	21.277	17.352	7.806
C_1	8.965	0.223	8.246	0.833	7.336	0.184	9.849	0.864	22.195	20.967	16.273	3.566
C_2	6.491	−0.085	8.246	0.874	5.075	−0.062	10.000	0.877	27.894	36.232	17.538	0.342
C_3	7.063	−0.071	7.071	0.526	5.212	−0.077	8.485	0.597	35.514	7.712	16.666	11.960
C_4	6.509	−0.141	8.544	0.927	5.371	−0.105	10.050	0.888	21.195	34.670	14.984	4.323
C_5	6.266	0.122	7.616	0.595	5.071	0.128	9.220	0.685	23.564	5.066	17.395	13.220
C_6	6.800	−0.094	8.062	0.855	5.145	−0.148	9.849	0.911	32.170	36.995	18.140	6.139
C_7	5.740	0.028	7.810	0.685	4.655	0.024	9.849	0.807	23.313	14.583	20.700	15.097
C_8	5.900	0.075	7.071	0.500	5.030	0.092	8.485	0.571	17.284	18.033	16.666	12.404
C_avg.	6.717	0.007	7.833	0.724	5.362	0.005	9.473	0.775	25.391	21.782	17.295	8.381

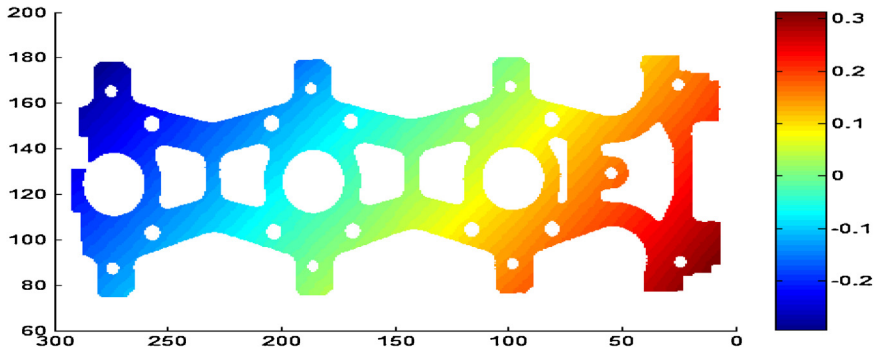

Fig. 16. The height map of the cylinder head.

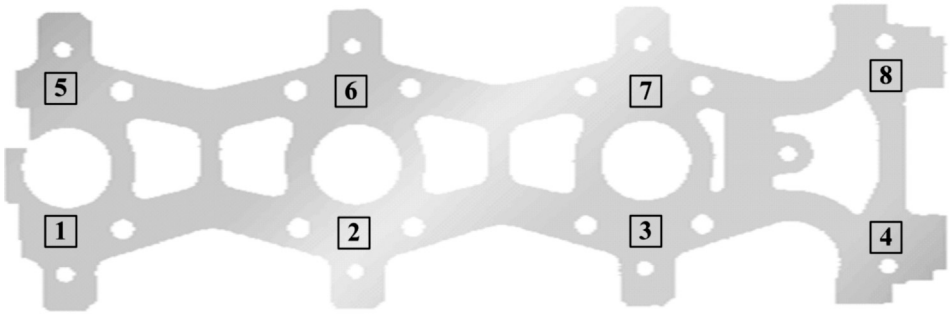

Fig. 17. Eight locations selected from this surface.

Table 3
Comparison of amplitude parameters.

Unit: μm	Shearlet filter			Gaussian filter			Difference (%)		
	S_a	S_q	S_t	S_a	S_q	S_t	S_a	S_q	S_t
L_1	0.051	0.068	0.860	0.053	0.069	0.668	4.307	1.594	28.704
L_2	0.051	0.066	0.557	0.054	0.068	0.547	4.664	2.504	1.847
L_3	0.052	0.069	0.782	0.056	0.073	0.743	7.348	4.945	5.289
L_4	0.057	0.073	0.687	0.059	0.075	0.598	3.735	2.394	14.890
L_5	0.050	0.067	0.776	0.054	0.070	0.612	7.778	4.585	26.892
L_6	0.059	0.081	1.005	0.065	0.086	0.860	8.756	5.794	16.913
L_7	0.056	0.074	0.814	0.061	0.080	0.811	8.264	7.035	0.382
L_8	0.062	0.082	0.796	0.068	0.088	0.774	8.944	6.818	2.776
Average	0.055	0.073	0.785	0.059	0.076	0.702	6.725	4.459	12.212

applied by combining the four highest levels (levels 3–6) of details as roughness ($j_r = 3$), the two lowest levels of details (levels 1–2) as waviness ($j_w = 1$) and approximations at level 1 as form, the results can be obtained as shown in Fig. 19. Likewise, the Gaussian filter is also implemented on this surface ($\lambda_{xc} = \lambda_{yc} = 0.01 \times (2^{3/2})^4 = 0.64$ mm) and the results are shown in Fig. 20. Then the surface texture parameters presented in Case Study I are also calculated using the roughness data obtained by the two methods respectively. Tables 3 and 4 list all the surface texture parameters using these two methods and the differences between them. It can be found in Table 3 that the average differences are about 7% in S_a values, 5% in S_q values and 12% in S_t values. Table 4 shows that the average differences of the shape and space parameters between the two methods are less than 20% in general.

Table 4
Comparison of shape and space parameters.

	Shearlet filter				Gaussian filter				Difference (%)			
	S_{ku}	S_{sk}	S_{al}	S_{tr}	S_{ku}	S_{sk}	S_{al}	S_{tr}	S_{ku}	S_{sk}	S_{al}	S_{tr}
L_1	4.723	−0.029	8.485	0.849	3.790	−0.037	10.296	0.646	24.810	22.581	17.583	31.286
L_2	3.649	−0.054	7.810	0.395	3.196	−0.079	9.434	0.296	14.166	31.258	17.212	33.097
L_3	4.632	−0.084	8.062	0.475	3.983	−0.097	9.900	0.426	16.293	13.669	18.559	11.657
L_4	3.811	−0.032	8.485	0.667	3.328	−0.040	9.900	0.564	14.504	19.799	14.286	18.188
L_5	4.418	−0.022	8.544	0.804	3.630	−0.017	10.630	0.607	21.700	26.437	19.624	32.487
L_6	5.331	−0.180	7.810	0.316	4.265	−0.157	9.900	0.279	24.995	14.522	21.105	13.042
L_7	4.445	−0.198	8.485	0.429	4.188	−0.219	10.000	0.388	6.146	9.332	15.147	10.435
L_8	4.098	0.018	8.602	0.714	3.653	0.014	10.630	0.622	12.193	23.239	19.076	14.855
Average	4.389	−0.073	8.286	0.581	3.754	−0.079	10.086	0.479	16.851	20.105	17.824	20.631

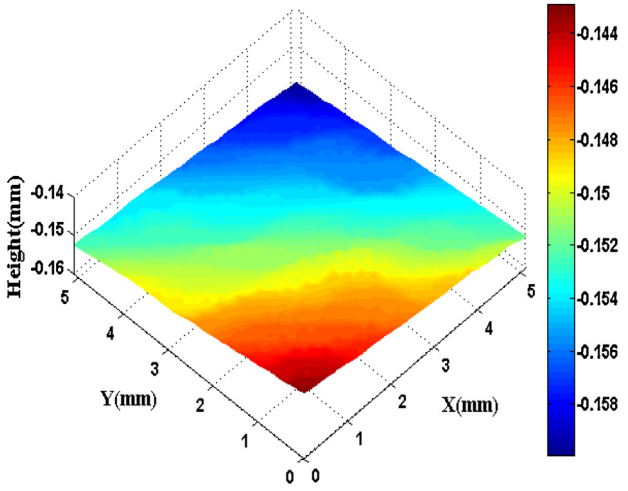

Fig. 18. Selected surface from Location 1.

5.3. Case Study III

The third engineering surface is the surface of a pump valve plate which is also produced by milling, and the height map of this surface is shown in Fig. 21. The experimental process of this surface is completely the same as that of the second surface except that there are six locations selected from this surface (see Fig. 22).

Likewise, Table 5 presents the comparison of computed amplitude surface parameters using shearlet filter and Gaussian filter respectively. The last three columns of it show that the average differences of amplitude parameters are 8–12%. Table 6 presents the comparison of computed shape surface parameters and space surface parameters, and it can be found that the differences of the shape and space parameters between the two methods are 15–25%. Taking the two cases in Sections 5.2 and 5.3 into consideration, a conclusion can be drawn that the differences of amplitude parameters obtained by the two methods are around 10% while the differences of the shape and space parameters are around 20%. This conclusion is approximate to that of Case Study I, which demonstrates that the differences between the surface parameters

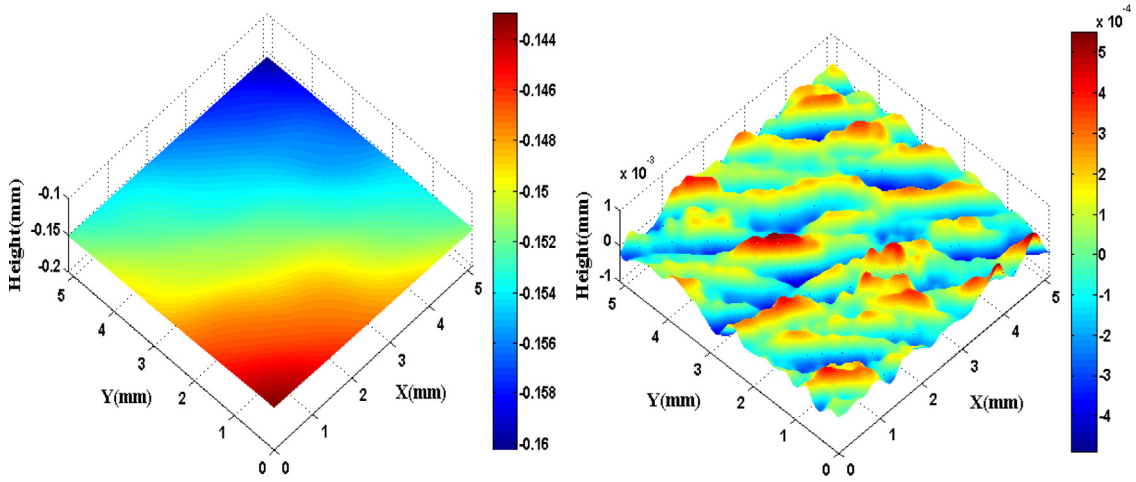

(a) Form

(b) Waviness surface

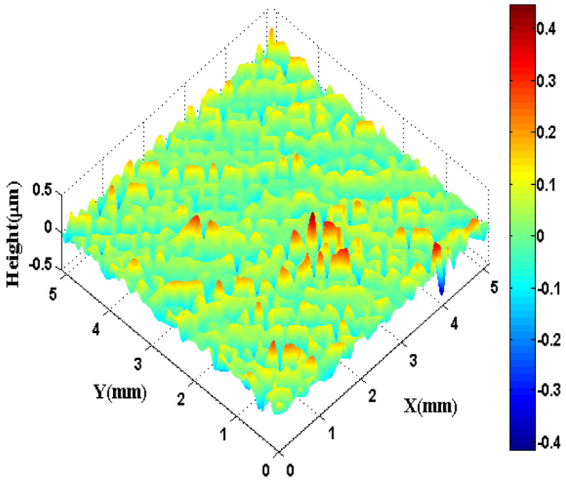

c) Roughness surface

Fig. 19. Surface texture decomposition with shearlet filter.

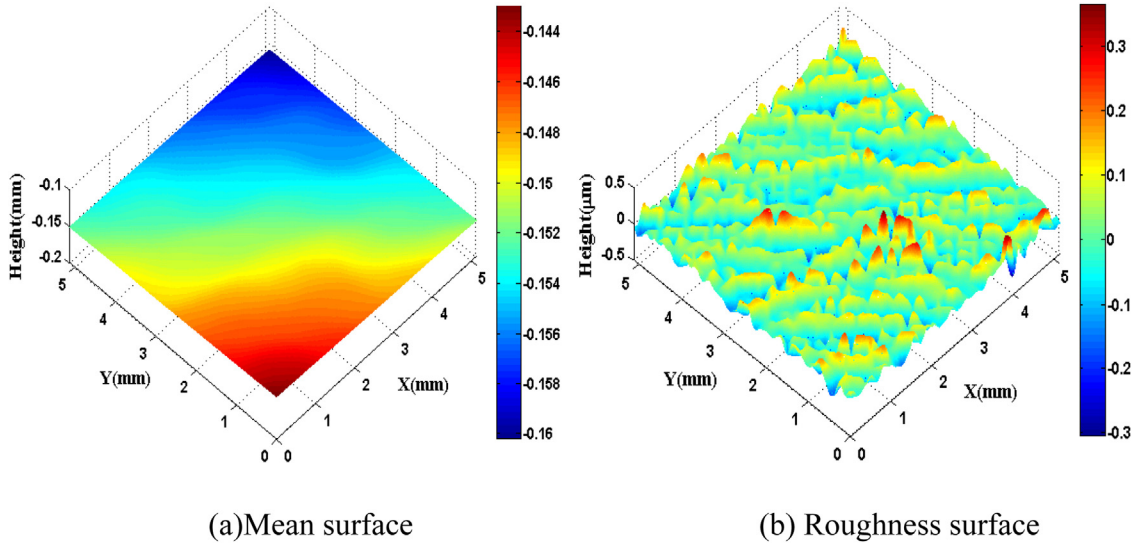

Fig. 20. Surface texture decomposition with Gaussian filter.

Table 5
Comparison of amplitude parameters.

Unit: μm	Shearlet filter			Gaussian filter			Difference (%)		
	S_a	S_q	S_t	S_a	S_q	S_t	S_a	S_q	S_t
L_1	0.036	0.047	0.524	0.041	0.052	0.437	12.099	9.770	19.876
L_2	0.043	0.058	0.663	0.049	0.064	0.628	12.500	9.798	5.654
L_3	0.037	0.049	0.512	0.041	0.053	0.468	10.412	7.590	9.470
L_4	0.037	0.049	0.525	0.041	0.053	0.539	11.165	8.835	2.579
L_5	0.038	0.051	0.499	0.042	0.055	0.482	9.953	8.015	3.571
L_6	0.039	0.052	0.778	0.043	0.056	0.633	9.602	6.115	22.926
Average	0.038	0.051	0.583	0.043	0.055	0.531	10.955	8.354	10.679

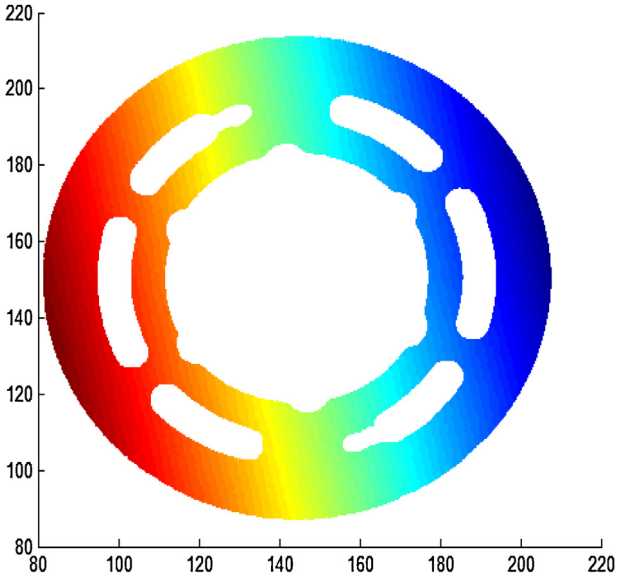

Fig. 21. The height map of the pump valve plate.

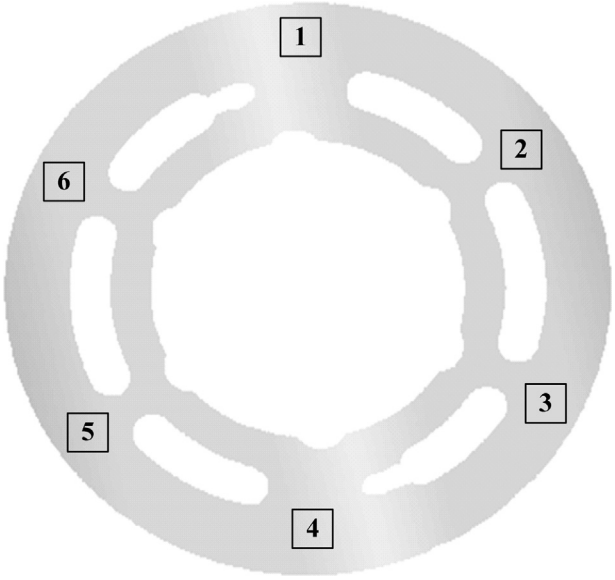

Fig. 22. Six locations selected from this surface.

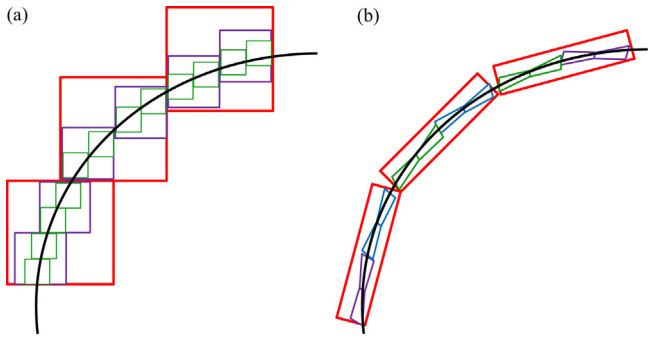

Fig. 23. The representation of a plane curve using (a) 2D DWT and (b) shearlets.

through Gaussian filter and shearlet filter are within a reasonable range.

5.4. Discussions of properties

Compared with the traditional wavelets, shearlets have the following properties which make it more appropriate in the filtering of 3D engineering surfaces.

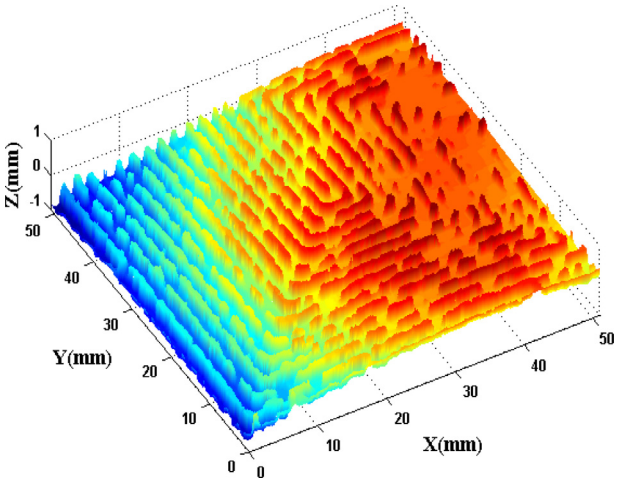

Fig. 24. Raw PCB surface.

(1) Shearlets not only maintain the multi-resolution and time-frequency localization characteristics of wavelets, but also perform well in capturing the geometric regularity along singularities of surfaces due to their anisotropic supports.

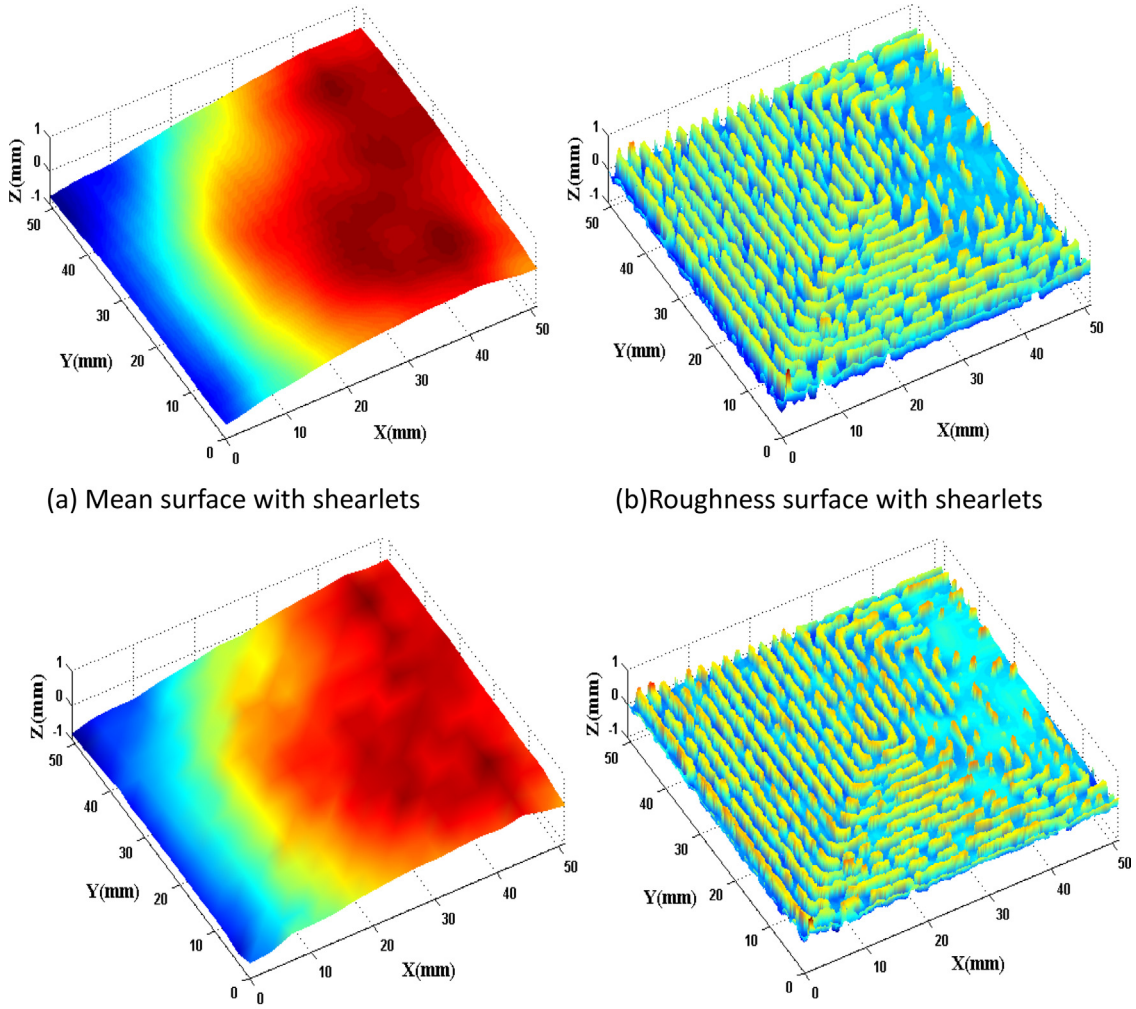

Fig. 25. Comparison of shearlet and 2D DWT for the separation of the PCB surface.

Table 6
Comparison of shape and space parameters.

	Shearlet filter				Gaussian filter				Difference (%)			
	S_{ku}	S_{sk}	S_{al}	S_{tr}	S_{ku}	S_{sk}	S_{al}	S_{tr}	S_{ku}	S_{sk}	S_{al}	S_{tr}
L_1	4.333	0.032	8.944	0.640	3.491	0.041	10.770	0.504	24.128	22.794	16.954	27.114
L_2	5.095	0.039	8.544	0.540	4.238	0.031	10.198	0.408	20.211	26.885	16.219	32.483
L_3	4.289	−0.209	8.246	0.592	3.511	−0.207	10.198	0.504	22.156	1.162	19.139	17.554
L_4	4.337	0.012	8.246	0.478	3.840	0.015	10.050	0.377	12.951	19.595	17.947	26.845
L_5	4.464	−0.033	8.246	0.566	3.844	−0.036	10.198	0.471	16.107	7.778	19.139	20.199
L_6	5.751	−0.154	8.246	0.633	4.235	−0.117	10.050	0.558	35.793	31.990	17.947	13.453
Average	4.711	−0.052	8.412	0.575	3.860	−0.046	10.244	0.470	21.891	18.367	17.891	22.941

(2) Shearlets exhibit highly directional sensitivity. Compared with 2D DWT, which only has three directions (horizontal, vertical and diagonal), shearlets are unconstrained on the numbers of directions, which make it directional sensitive in recognizing surface textures.
(3) Shearlets are able to provide representations of larger and higher dimensional data that are sparse (that is, only a few terms of the representations are sufficient to accurately approximate the data) and computationally efficient.

The properties (1) and (3) can be illustrated vividly through Fig. 23. It shows the process of representing one plane curve by wavelets and shearlets, respectively. The 2D DWT have square supports, and these square supports have different sizes in different scales. Then the representation of the plane curve is actually equal to the process of using "points" to approximate the plane curve. When the scale becomes finer, the number of none-zero wavelet coefficients will grow exponentially, which makes it unable for wavelets to get the sparse representation of the function. In contrast, shearlets have elongated supports that can approximate the plane curve with the least amount of coefficients. Since shearlets have anisotropic supports, they can capture geometric smoothness of the curves efficiently, whereas wavelets are only good at capturing point discontinuities. Additionally, NSST is adopted in this paper, which not only maintains the merits of shearlets, but also possesses the property of fully shift-invariance. Lacking of shift-invariance will lead to the distortion of reconstructed images at different scales after filtering, which is faced by DWT (see Fig. 5(c)). However, NSST is free from this problem and therefore it is suitable to handle complex engineering surfaces.

The role of property (2) is embodied in the separation of engineering surfaces with directional features like lines and curves. To demonstrate this, a worn printed circuit board (PCB) is used for experiment and part of its surface is selected as input of the filtering methods, which is shown in Fig. 24. It can be seen that there are many lines and curves on this PCB surface. Both 2D DWT and shearlet filter are used to separate this surface, and the results are shown in Fig. 25. It can be found that the mean surface (low-pass components) obtained by shearlet filter is closer to the form of the raw PCB surface than that obtained by 2D DWT. Besides, the roughness surface (high-pass components) obtained by shearlet filter contains more detail information of texture compared with the one obtained by 2D DWT. Using shearlet filter, all the detail features are extracted precisely and the PCB surface form is preserved without any distortion.

6. Conclusions

This paper has developed a shearlet-based separation method of 3D engineering surface using high definition metrology. A 3D engineering surface is decomposed into different sub-bands of coefficients with NSST, and these coefficient sub-bands include high-frequency details and low-frequency approximations. The surface components are reconstructed by INSST and surface roughness, waviness and form are obtained by combing different frequency components based on the cut-off wavelengths. The performance of shearlet filter is validated by simulated surface data and real-world 3D surface data using high definition metrology. Also several 3D surface texture parameters are computed respectively based on the roughness surfaces and compared with those of Gaussian filter. The comparison results have illustrated the effectiveness of shearlet filter. Additionally, considering its ability of multi-resolution, good time-frequency localization, highly directional sensitivity and shift-invariant property, shearlets are expected to be superior to the current ISO standardized Gaussian filter and wavelet filters like DWT. Shearlets can be a powerful tool in 3D surface texture analysis in the future, when much finer analysis of engineering surfaces becomes necessary.

Acknowledgements

The authors greatly acknowledge the editor and the reviewers for their valuable comments and suggestions that have led to a substantial improvement of the paper. This work was supported by the National Natural Science Foundation of China (Grant No. 51275558), National Key Science and Technology Research Program of China (Grant No. 2014ZX04015-021), and Shanghai Rising-Star Program (Grant No. 13QA1402100).

References

[1] Raja J, Muralikrishnan B, Fu S. Recent advances in separation of roughness, waviness and form. Precis Eng 2002;26:222–35.
[2] ISO 11562. Geometrical product specification (GPS)—surface texture: profile method—metrological characteristics of phase correct filters. Geneva: International Organization for Standardization; 1996.
[3] Brinkmann S, Bodschwinna H, Lemke H-W. Accessing roughness in three-dimensions using Gaussian regression filtering. Int J Mach Tools Manuf 2001;41:2153–61.
[4] Krystek M. Form filtering by splines. Measurement 1996;18:9–15.
[5] Goto T, Miyakura J, Umeda K, Kadowaki S, Yanagi K. A robust spline filter on the basis of L_2-norm. Precis Eng 2005;29:157–61.
[6] Srinivasan V. Discrete morphological filters for metrology. In: Proceedings of the 6th ISMQC symposium on metrology for quality control in production. 1998. p. 623–8.
[7] Chen X, Raja J, Simanapalli S. Multi-scale analysis of engineering surfaces. Int J Mach Tools Manuf 1995;35:231–8.
[8] Chen Q, Yang S, Li Z. Surface roughness evaluation by using wavelets analysis. Precis Eng 1999;23:209–12.
[9] Muralikrishnan B, Raja J. Computational surface and roundness metrology. Springer; 2009.
[10] Fu S, Muralikrishnan B, Raja J. Engineering surface analysis with different wavelet bases. J Manuf Sci Eng 2003;125:844–52.
[11] Jiang X, Blunt L, Stout K. Development of a lifting wavelet representation for surface characterization. Proc R Soc Lond Ser A: Math Phys Eng Sci 2000;456:2283–313.
[12] Josso B, Burton DR, Lalor MJ. Frequency normalised wavelet transform for surface roughness analysis and characterisation. Wear 2002;252:491–500.
[13] Huang Z, Shih AJ, Ni J. Laser interferometry hologram registration for three-dimensional precision measurements. J Manuf Sci Eng 2006;128:1006–13.
[14] Blunt L, Jiang X. Advanced techniques for assessment surface topography: development of a basis for 3D surface texture standards "Surfstand". Elsevier; 2003.
[15] ASME B46.1 Surface texture (surface roughness, waviness, and lay). 2002.

[16] Liao Y, Stephenson DA, Ni J. Multiple-scale wavelet decomposition, 3D surface feature exaction and applications. J Manuf Sci Eng 2012;134:011005.
[17] Chen M, Pang Q, Wang J, Cheng K. Analysis of 3D microtopography in machined KDP crystal surfaces based on fractal and wavelet methods. Int J Mach Tools Manuf 2008;48:905–13.
[18] Zeng W, Jiang X, Scott P. Metrological characteristics of dual-tree complex wavelet transform for surface analysis. Meas Sci Technol 2005;16:1410.
[19] Guo K, Labate D. Optimally sparse multidimensional representation using shearlets. SIAM J Math Anal 2007;39:298–318.
[20] Easley G, Labate D, Lim W-Q. Sparse directional image representations using the discrete shearlet transform. Appl Comput Harmon Anal 2008;25:25–46.
[21] Wang L, Li B, Tian LF. A novel multi-modal medical image fusion method based on shift-invariant shearlet transform. Imaging Sci J 2013;61:529–40 (12).
[22] Danti A, Poornima K. Face recognition using shearlets. In: Proceedings of the 7th IEEE international conference on industrial and information systems. IEEE; 2012. p. 1–6.
[23] Mallat S. A wavelet tour of signal processing. Academic Press; 1999.
[24] Da Cunha AL, Zhou J, Do MN. The nonsubsampled contourlet transform: theory, design, and applications. IEEE Trans Image Process 2006;15:3089–101.
[25] http://www.coherix.com
[26] Wang M, Xi L, Du S. 3D surface form error evaluation using high definition metrology. Precis Eng 2014;38(1):230–6.
[27] Thomas T, Charlton G. Variation of roughness parameters on some typical manufactured surfaces. Precis Eng 1981;3:91–6.